

Anisotropic magnetodielectric coupling in layered antiferromagnetic FePS₃Anudeepa Ghosh,¹ Magdalena Birowska,² Pradeepta Kumar Ghose,¹ Miłosz Rybak,³ Sujan Maity,¹ Somsubhra Ghosh,¹ Bikash Das,¹ Koushik Dey,¹ Satyabrata Bera,¹ Suresh Bhardwaj,⁴ Shibabrata Nandi,^{5,6} and Subhadeep Datta^{1,*}¹*School of Physical Sciences, Indian Association for the Cultivation of Science,**2A & B Raja S. C. Mullick Road, Jadavpur, Kolkata 700032, India*²*Faculty of Physics, Institute of Theoretical Physics, University of Warsaw, Pasteura 5, 02093, Warsaw, Poland*³*Department of Semiconductor Materials Engineering, Faculty of Fundamental Problems of Technology, Wrocław University of Science and Technology, Wybrzeże Wyspiańskiego 27, PL-50370 Wrocław, Poland*⁴*UGC-DAE Consortium for Scientific Research, University Campus, Khandwa Road, Indore 452001, India*⁵*Forschungszentrum Jülich GmbH, Jülich Centre for Neutron Science (JCNS-2) and Peter Grünberg Institut (PGI-4), JARA-FIT, 52425 Jülich, Germany*⁶*RWTH Aachen, Lehrstuhl für Experimentalphysik IVc, Jülich-Aachen Research Alliance (JARA-FIT), 52074 Aachen, Germany*

(Received 4 August 2022; revised 13 June 2023; accepted 3 August 2023; published 18 August 2023)

We report anisotropic magnetodielectric coupling in layered van der Waals antiferromagnetic FePS₃ (Néel temperature $T_N \sim 120$ K) with perpendicular anisotropy. Above T_N , while the dielectric response function along the c axis shows frequency-dependent relaxations, in-plane data is frequency independent and reveals a deviation from phonon-anharmonicity in the ordered state, thereby implying a connection to spin-phonon coupling known to be indicative of onset of magnetic ordering. At low temperature (below 40 K), atypical anomaly in the dielectric constant is corroborated with temperature-dependent dc and ac susceptibility. The magnetodielectric response across this anomaly differs significantly for both in-plane and out-of-plane cases. We have explained this in terms of preferential orientation of magnetic antiferromagnetic zigzag alignment, implied by the in-plane structural anisotropy as confirmed by *ab initio* calculations. Controlling the relative strength of magnetodielectric coupling with magnetic anisotropy opens a strategy for tracking subtle modifications of structures, such as in-plane anisotropy, with potential applications for spintronic technologies.

DOI: [10.1103/PhysRevB.108.L060403](https://doi.org/10.1103/PhysRevB.108.L060403)**I. INTRODUCTION**

Multifunctional devices based on spin-charge coupling involve low-frequency shifts of dielectric constant with magnetic ordering [1]. Additionally, the presence of the magnetic anisotropy (MA) may drive the exotic spin textures and, in turn, lead to electric field control of the magnetic ground state [2,3]. Two-dimensional (2D) van der Waals (vdW) magnetic materials are of particular interest due to the presence of MA originating from the interaction between the magnetic moments and the crystal field. Also, these materials indicate a high degree of stability in the long-range spin order and may be described using suitable spin Hamiltonians of the Heisenberg, XY, or Ising type. Moreover, recent reports have suggested effective interactions between magnetization and electric polarization in 2D magnets [4–6]. Exploring different routes to MD coupling, such as complex spin structures, magnetostructural, and magnetoelastic effects, has become important from a fundamental point of view as well as device applications [7–14].

Other than charge-/spin-transport measurements, the co-existence of electric and magnetic orders in a few-layer antiferromagnet (AFM) can be detected from phonon anomalies *via* μ -Raman spectroscopy or optical second harmonic generation. However, direct probing of a dielectric constant

with varying temperature, frequency, and magnetic-field parameters in transition-metal (M) trichalcogenides (MPX_3 , $X = S, Se$), in their bulk forms, is still largely missing from the literature. The vdW gaps in relatively air-stable MPX_3 ($\sim 2\text{--}3$ Å) host interstitial sites that have shown to facilitate intercalation of guest ions [15,16] and can thus provide hopping sites in the out-of-plane direction. This is absent in the in-plane direction since it is constituted of strong covalent bonds. In the conventional parallel-plate-capacitor measurement scheme, anisotropic lattice and spin texture in these magnetic insulators result in contrasting dielectric properties with different charge carrier transport mechanisms in the in-plane ($\mathbf{E} \parallel c\text{-axis}$) and out-of-plane ($\mathbf{E} \perp c\text{-axis}$) directions.

Here, we present a comprehensive low-temperature dielectric spectroscopy of a layered AFM FePS₃ with $T_N \sim 120$ K. The dielectric function measured along the c axis is frequency independent in the AFM phase but shows the onset of dielectric relaxations above T_N . On the other hand, the in-plane function remains frequency independent throughout and shows deviations from the usual anharmonic behavior at T_N which can be correlated to the spin-phonon coupling from our previous study [17]. The out-of-plane relaxations have corroborated with temperature-dependent dc conductivity and analyzed in terms of the small polaron (SP) hopping model. A distinct anomaly is observed in the dielectric constant around 50 K and is also reflected in ac magnetic susceptibility. These have explained in terms of preferential orientation of the

*Corresponding author: sspsdd@iacs.res.in

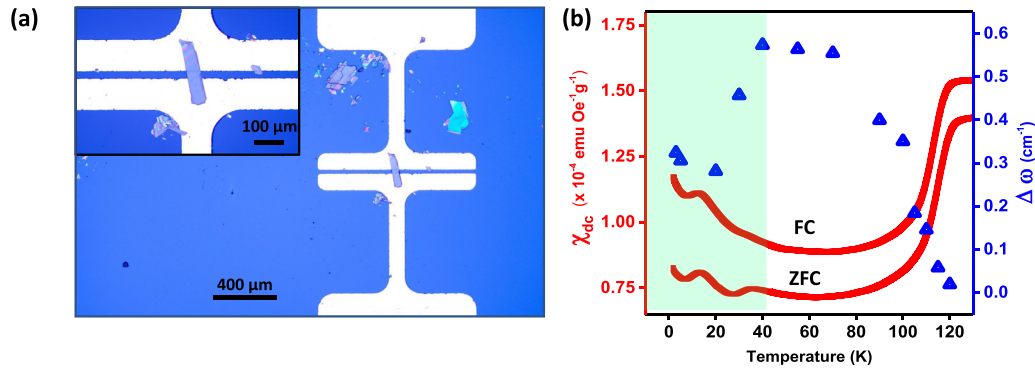


FIG. 1. Iron phosphorus trisulfide (FePS_3): (a) Optical image showing two probes with a FePS_3 flake stamped on it. Inset shows zoomed-in image of the flake. (b) Low-temperature portion (at and below T_N) of dc susceptibility taken at a field of 500 Oe plotted against temperature on the left axis. Right axis shows the deviation from anharmonicity ($\Delta\omega$) for the Raman peak at 285 cm^{-1} plotted as a function of temperature. The former shows a distinct upturn below 40 K much below Néel temperature $\sim 120\text{ K}$ at which antiferromagnetic ground state is established. The latter shows a decrease in $\Delta\omega$ around 40 K.

antiferromagnetic zigzag (AFM-z) phase alignment within the plane, enabled by the in-plane structural anisotropy, facilitated by distortion of lattice parameters at low temperatures, and supported by theoretical considerations. A contrasting phenomenon is observed in the magnetodielectric response across this anomaly between the out-of-plane and in-plane directions with spin-phonon correlation-assisted magnetodielectric coupling showing up for the in-plane case.

II. SAMPLE PREPARATION AND MEASUREMENT

Single crystals of FePS_3 were grown by the chemical vapor transport method, characterized and studied *via* x-ray diffraction (XRD), energy dispersive x-ray analysis, dc and ac susceptibility. Low-temperature dielectric spectroscopy with varying frequency and magnetic field were performed following the parallel-plate geometry for the in-plane and out-of-plane measurements on exfoliated bulk material [Fig. 1(a)]. For computational studies, the static dielectric properties were calculated by means of density functional perturbation theory implemented in the VASP software. Details of the crystal growth, measurement schemes, and computational studies are given in the Supplemental Material (SM) [18].

III. RESULTS AND DISCUSSION

A. Dielectric spectroscopy

1. Region around the Néel temperature

The out-of-plane ($\mathbf{E}||c$) dielectric constant (ϵ') of FePS_3 as a function of temperature for various frequencies is shown in Fig. 2(a). In the AFM phase, below T_N , ϵ' is almost frequency and temperature independent, representing the static part of the dielectric constant due to the electronic and ionic contributions [38].

As the temperatures is increased, in the paramagnetic (PM) phase, a rapid increase in ϵ' is observed with the onset of frequency-dependent dielectric relaxations. This also manifests as peaks in the loss factor $\tan \delta$ (not shown here) which shows wide shifts towards higher temperature with increasing frequency, indicating thermally activated relaxation mechanism [39]. Two different types of relaxations in the PM state for the given temperature window can be identified, as marked

by A and B in Fig. 2(a). In the frequency range being probed, the relaxations can either arise from Debye/Debye-like relaxation or from the charge accumulation near boundaries, otherwise called Maxwell-Wagner (MW) relaxations [9,38]. The slope calculated from the $\log(\epsilon'')$ vs $\log(f)$ plot is found to be (-1) in the B region (see SM [18]), suggesting the presence of the MW relaxation [9]. For a vdW material like FePS_3 , the constituent layers in the bulk along the out-of-plane direction are separated by vdW gaps, which may lead to interfacial charge accumulation between layers.

The MW relaxation model, however, fails to fit the data in region A (see Fig. 2(a) and SM [18]). This interim temperature regime (region A) was fitted with the Debye-like model (see SM [18]) with a characteristic relaxation time and can be attributed to the response of the polar microregions in field \mathbf{E} . Accordingly, the combined MW and Debye-like model explains the data over the entire temperature regime in A and B. For Debye-like relaxation, the relaxation time (τ_0) and activation energy (\bar{E}) determined from the Arrhenius relation (see SM [18]) were found to be $1.5 \times 10^{-7}\text{ s}$ and 219 meV, respectively. The large relaxation time indicates a hopping-type conduction of quasiparticle such as SPs through interstitial sites in vdW gaps [38,40]. Considering the nearest-neighbor (NN) SP hopping, the temperature-dependent dc resistivity [ρ_{dc}/T versus $1000/T$ plot in Fig. 2(b)] measured in the top-bottom configuration can be described by [40,41]

$$\rho = CT \exp\left(\frac{E_A}{k_B T}\right), \quad (1)$$

where E_A is the activation energy, k_B is Boltzmann's constant, and C is the prefactor. The activation energy calculated from the fit is 170 meV, which corroborates with that calculated from Arrhenius relation. The NN-SP model [Eq. (1)] fits well with the data for temperatures above 180 K but shows deviation below 180 K. Alternative mechanisms like Mott's variable range hopping (VRH) or Shklovskii-Efros variable range hopping (ES-VRH) fail to fit the data in the temperature regime below 180 K [see inset of Fig. 2(b)] [42,43]. Considering the limiting case approximation, where SPs can penetrate to neighboring sites by the phonon-induced tunneling effect, the hopping-type transport becomes dominant for $T > 0.5\hbar\omega/k_B$ [38,44], where ω is the optical mode angular

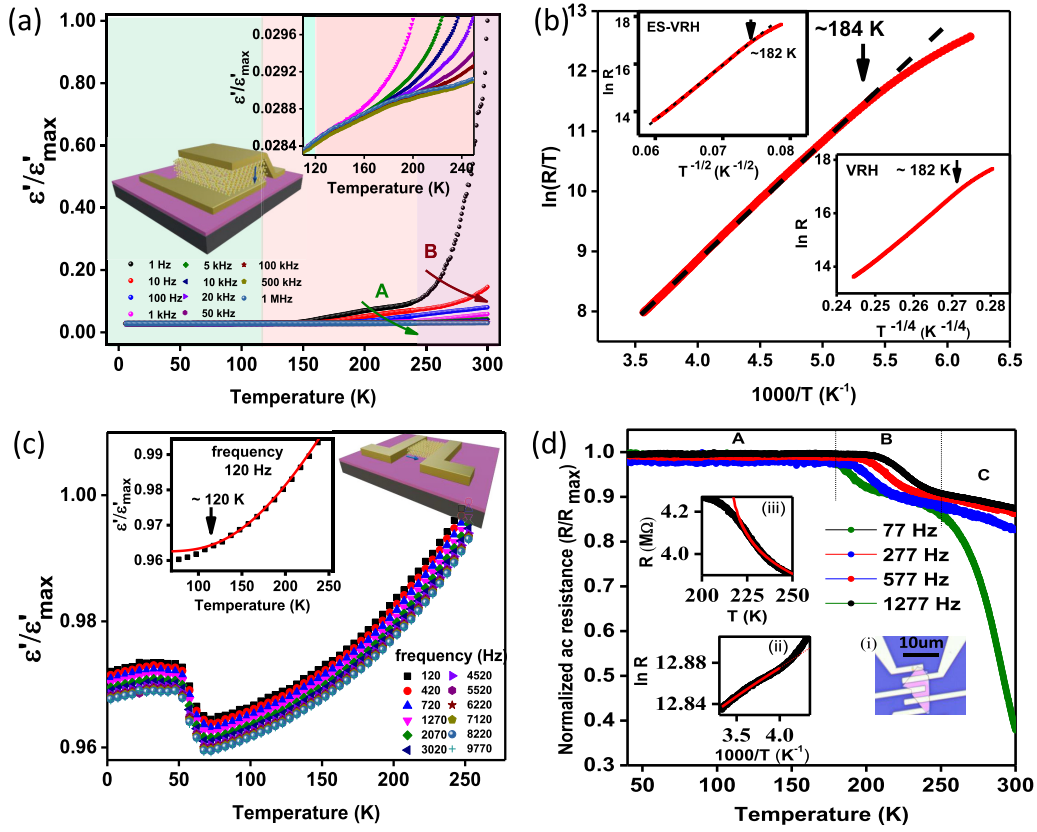


FIG. 2. Dielectric spectroscopy: (a) Temperature-dependent (3–300 K) measurement at different frequencies for out-of-plane geometry. Two different relaxation regions are marked as A and B. Inset shows the dispersion for higher frequencies in the intermediate temperature regime. (b) Arrhenius plot for out-of-plane resistance showing deviation at ~ 184 K. Similar deviation is seen in ES-VRH and VRH shown in top and bottom inset. (c) Temperature-dependent (3–250 K) measurement at different frequencies for in-plane geometry. Inset shows normalized dielectric permittivity with Einstein fit showing deviation around 120 K. (d) Temperature-dependent normalized in-plane AC resistance of FePS₃ bulk flake [see inset (i)] with fitting of resistivity in two different temperature ranges [250–300 K in inset (ii) and 220–250 K in inset (iii)].

frequency. Below $T \approx 180$ K lies the non-Arrhenius regime, dominated by tunneling transport of polarons, which puts a figure on vibrational spin-phonon coupled Raman-active bulk mode (ω) at 250 cm^{-1} , reported in our previous study [17].

The in-plane dielectric constant shows no frequency-dependent dielectric relaxations for the entire temperature and frequency range [see Fig. 2(c)], which asserts the effect of vdW gaps in the out-of-plane direction. One may note that the samples used in this study are pristine bulk flakes and well stamped *via* micromanipulation technique. The temperature-dependent low-frequency dielectric permittivity [$\varepsilon_0(T)$] of an insulator without any structural, ferroelectric, or magnetic phase transition is characterized by an Einstein-type function as [1,45]

$$\varepsilon_0(T) = \varepsilon_0(0) + \frac{A}{\exp\left(\frac{\hbar\omega^*}{k_B T}\right) - 1}, \quad (2)$$

where $\varepsilon_0(0)$ and A are constants and ω^* is the frequency of the effective infrared (IR) active optical phonon with a dominant dielectric strength at zero temperature. A frequency value of $\approx 431 \text{ cm}^{-1}$ has been predicted as a strong IR active mode in bulk FePS₃ in an earlier report by Joy and Vasudevan [46] and is thus chosen as ω^* , which fits well with the experimental

data for $f = 120$ Hz [inset Fig. 2(c)]. The in-plane dielectric data deviates from the anharmonic fit around $T_N \approx 120$ K, similar to Raman spectroscopic studies [17], indicating the influence of spin-phonon coupling in FePS₃. The temperature variations of normalized in-plane ac resistance (R/R_{max}) show three different regions marked as A, B, and C [see inset Fig. 2(d)]. At lower temperatures, below 120 K (region A), temperature-independent resistance for all frequencies can be observed. At higher temperatures, a sudden drop in resistance has been recorded for all the measured frequencies (region B). However, the drop in resistance has been found to start from higher temperatures for higher frequencies. Figure 2(d)(ii) shows $\ln R$ versus $1000/T$ plot from 250–300 K (region C), which agrees well with the Arrhenius law $R \sim \exp(E_a/2k_B T)$ with the activation energy (E_a) as 81.6 meV [47]. However, below 250 K, a pronounced upturn in the resistivity data is clearly seen from where the thermally activated Arrhenius model fails to explain the temperature variation of R . This upturn behavior can be explained by spin-charge scattering using the relation $\rho = A + B \ln(T_{\text{SF}}/T)$, where A and B are constants and T_{SF} is the temperature below which spin fluctuation starts [48]. Here, we incorporate the concept of spin fluctuations and spin-charge scattering to explain the resistivity upturn, as there is evidence of spin dynamics and

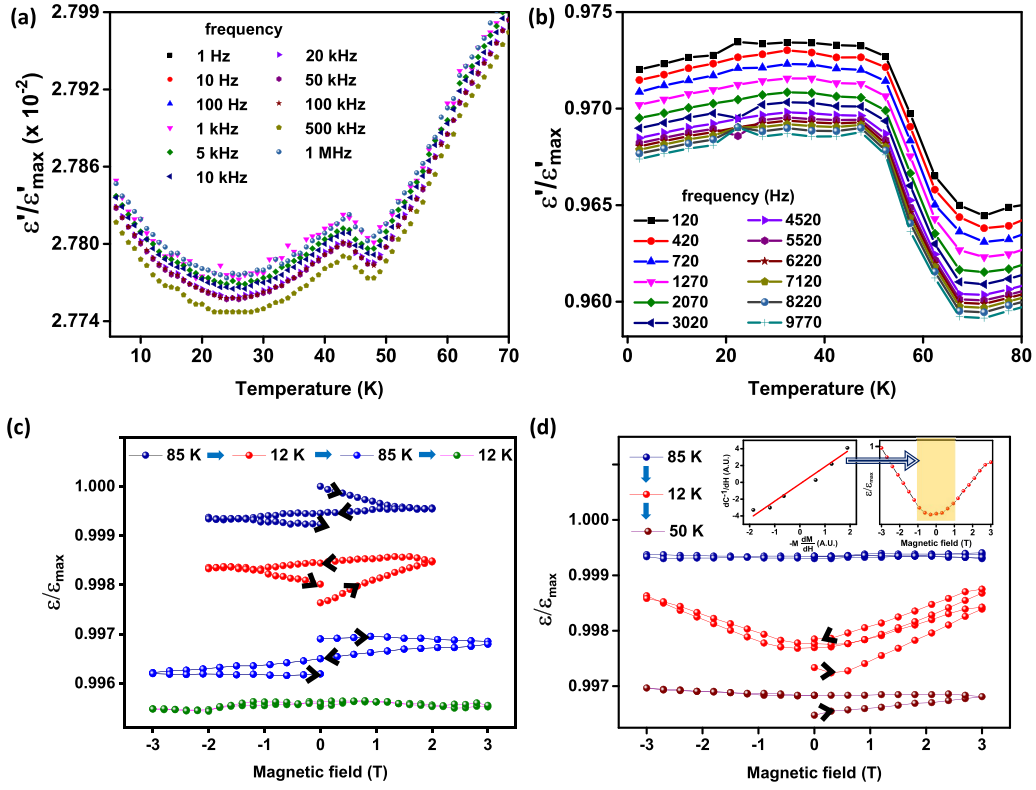


FIG. 3. (a) Magnetodielectric coupling: (a), (b) Dielectric spectra in the low-temperature region, (a) Out-of-plane measurements for different frequencies showing a kink around 50 K followed by a change in the nature of the curve below 40 K. (b) In-plane measurement showing a prominent jump at temperature around 50 K. (c), (d) Dielectric response as a function of magnetic field sweep, below and above the dielectric anomaly ~ 50 K. (c) Measurements with out-of-plane geometry were taken at selected temperatures in the following order: 85 K, 12 K, 85 K, 12 K. The nature of response on virgin sample shows a distinct difference between 85 K and 12 K, as shown by the navy and red plots. Even though the 85 K data reproduces, the response at 12 K is lost (see Sec. III A 1). (d) In-plane measurement has been taken consecutively at 85 K (navy), 12 K (red), 50 K (brown), which show no locking effect, and a prominent magnetodielectric coupling is observed at 12 K.

magnon polarons in this compound [49,50]. Interestingly, in this temperature range, frequency-dependent dielectric relaxation is also prominent [Fig. 2(a)]. The T_{SF} obtained from the fitting [Fig. 2(d)(iii)] is 213 K, associated with the onset of spin fluctuation. Below this temperature range, R/R_{\max} are found to increase slowly, which indicates the suppression of spin-charge scattering. Also, several magnetic and dielectric anomalies can be observed to present which do not have much influence on temperature variation of resistivity [51].

2. Region around 50 K

A close inspection of the low-temperature dielectric data reveals a frequency-independent anomaly in ϵ' around ~ 50 K, reflected as a sudden jump in both out-of-plane [see Fig. 3(a)] and in-plane [see Fig. 3(b)] geometries. It is noteworthy that the characteristic Raman modes unveil an unusual downturn at ~ 40 K in the deviation from phonon anharmonicity ($\Delta\omega$), where $\Delta\omega$ a signature of the strength spin-phonon coupling arising at T_N [see Fig. 1(b)] [17]. Moreover, the magnetization data reflects a similar anomaly where χ_{dc} shows an upturn from the AFM ground state below $T < 40$ K [Fig. 1(b)]. The anomaly in ϵ' is usually correlated to magnetic phase transition [2,12,52] or ferroelectric ordering [53–55]. Note that magnetic field induced quantum fluctuation in AFM at

low temperature can also trigger such anomaly but does not match well with the scale ($\Delta\epsilon$) (discussed in the SM [18]). However, a displacive-type ferroelectric transition, especially in the out-of-plane case, might be a possibility [56].

B. Magnetodielectric response

We demonstrate anisotropic magnetodielectric response in FePS₃ in magnetic field space (\mathbf{H}) applied parallel to the c axis in FePS₃ for both in-plane and out-of-plane configurations. For the out-of-plane case, the manner in which applied magnetic fields change the dielectric response differs significantly above and below the dielectric anomaly seen around 50 K. Figure 3(c) shows the change in dielectric permittivity when the magnetic field is gradually swepted between 0 T and ± 2 T. The frequency is set to 100 kHz such that space-charge artifacts, contributing to magnetodielectricity, can be avoided. The first measurement taken at 85 K (navy) shows a continuous decrease in permittivity with an increase and subsequent decrease in magnetic field. There is a change of $\sim -0.08\%$ between the initial and final value after one complete cycle. Next, the temperature is lowered to 12 K and another cycle is taken (red). There is a marked change in the nature of dielectric response wherein the permittivity initially increases rapidly when field changes from 0 T to 2 T but thereafter

decreases from 2 T to -2 T and continues to decrease from -2 T to 0 T. The cycle is hysteric and the maximum change in capacitance is $\sim +0.08\%$. Next, the temperature is increased back to 85 K, where the initial nature of the curve is reproduced even with increase in magnetic field to ± 3 T. However, when the cycle is subsequently repeated at 12 K, the change in permittivity is now negligible ($\sim 0.009\%$). The curve loops onto itself with increasing and decreasing field and the initial behavior, seen in the virgin sample, is now lost. Even though the exact phenomenon behind such a distinctive difference in the magnetodielectric responses at 85 K and 12 K requires further studies, the observation demonstrates that the magnetic field induces an irreversible change in dielectric permittivity at low temperature. At lower temperature (\sim below 50 K), the temperature-induced structural frustration causes the micropolar regions to align differently than that at 85 K, such that the application of magnetic field causes locking of the moments which do not return to the original state even under a demagnetizing field.

For the in-plane case [Fig. 3(d)] taken at 100 kHz, however, the magnetodielectric response is significantly different than the out-of-plane case. There is no permanent locking effect and the measurements taken consecutively at 85 K (navy), 12 K (red), 50 K (brown), and 12 K (not shown) show a distinct magnetodielectric coupling which is most prominent at 12 K ($\sim +0.14\%$) and decreases with temperature, becoming negligible at 85 K. This can possibly be attributed to the spin-phonon coupling [1] observed in our previous report [17].

From Landau free-energy considerations, the variation of the inverse dielectric susceptibility function (which scales with inverse capacitance) can be expressed as [57]

$$\frac{d\chi^{-1}}{dH} = \sum_{i,j,k=0}^{\infty} D(i,j,k) i(i-1) P^{i-2} j \frac{dM}{dH} M^{j-1} \epsilon^k, \quad (3)$$

where χ is the dielectric susceptibility, $D(i,j,k)$ is a constant, P is the electric polarization, M is the magnetization, H is the magnetic field, and ϵ is the strain.

Careful examination of the derivative of the inverse dielectric susceptibility with magnetic field can give information about the coupling terms in the Landau free-energy expansion. If the $P^2 M^2$ coupling, which is always allowed by symmetry, is present in the material, then $\frac{d(1/C)}{dH}$ should be proportional to $M(\frac{dM}{dH})$ [57]. The first inset of Fig. 3(d) shows the plot of $\frac{d(1/C)}{dH}$ vs $-M(\frac{dM}{dH})$ at 12 K, which gives a straight line between ± 1 T [second inset Fig. 3(d)] but deviates thereafter.

With lowering of temperature, the distortion in lattice parameters (with the lengths of the a and b axis decreasing and increasing, respectively [58–61]), coupled with anisotropy, results in complex interactions within the domains, leading to frustration in the system below ~ 50 K and subsequent freezing. This explains the large temperature shift in χ' peaks and the anomalous jump in the dielectric spectra. This might lead to domain-wall motion or related dynamics at low temperatures which would be governed by the anisotropy constants [62]. The anomalous nature of χ' , showing two sets of frequency-dependent peaks, may point towards more than one domain-wall related phenomenon. Such temperature-

induced domain-wall movement has also been observed in other Ising-systems like CoNb_2O_6 [63]. Note that there have been theoretical predictions on the magnetic field and electrical current controlled domain-wall dynamics in 2D vdW magnets like CrI_3 , CrBr_3 , and MnPS_3 [64,65].

IV. THEORETICAL RESULTS

To understand the magnetodielectric measurements, we carried out the *ab initio* calculations of a bulk FePS_3 system. The magnetic ions (Fe) are arranged within the honeycomb lattice and exhibit AFM-z ordering. A previous temperature-dependent XRD study reported that the in-plane lattice constant ratio deviating from the hexagonal symmetry [58]. The latest XRD measurements demonstrated the nonequivalent Fe-S bond lengths within the FeS_6 octahedron, pointing to the existence of crystallographic in-plane anisotropy [66]. This might be a consequence of the symmetry breaking of the honeycomb structure with a further adjustment of the NN distance between the Fe atoms [67], implying a preferred direction of the AFM-z phase within the monolayer plane [66].

To elucidate the origin of the prominent jump around 50 K for the in-plane geometry [see Fig. 3(b)], we examine three plausible factors that might affect the dielectric properties of the bulk materials as presented in Fig. 4, namely, we examine the change of the lattice parameters with respect to elevating temperatures (model I), the change of the zigzag orientation within the monolayer frame (model II), and the impact of the magnetic phase (AFM-z, AFM-Néel) (model III). For all of these approaches, we examine the in-plane (ϵ_{\parallel}) and out-of-plane (ϵ_{\perp}) contributions of dielectric constant ϵ_0 . Note that ϵ_0 represents a macroscopic static response containing both the ionic (ϵ_{ion}) and electronic response (ϵ_{∞}) [18]. The stronger polarization is expected for covalent bonds (in-plane ones) and weaker for vdW-type bonding. Since the in-plane contributions are around five times larger than out-of-plane ones (see Fig. S6 and Table 1 in the SM), and the prominent jump is observed for the in-plane geometry, we only discuss the in-plane dielectric contributions below (for the details of out-of-plane contributions, see the SM [18]). To compare the theoretical results with experimental values, we define the relative dielectric constants as $\delta\epsilon_{\parallel} = (\epsilon_{\parallel} - \epsilon_{\text{ref}})/\epsilon_{\text{ref}}$, where ϵ_{\parallel} and ϵ_{ref} are particular and reference values of dielectric constants, respectively. The reference value is taken as a minimal value within the range under consideration. Now, we briefly explain each of the models.

As reported previously by XRD studies, the a/b lattice ratio exhibits strong temperature dependence [58]. In model I, we assumed the lattice parameter changes reported by Murayama *et al.* [58]. Note that the temperature was not included explicitly in our calculations and reflects only the lattice parameters measurements taken from 4 K upto 300 K [58]. Since the in-plane structural anisotropy was recently reported [66], the AFM-z phase exhibits preferred alignment within the layer, and its change might impact the dielectric properties. Thus, in model II we employ the change of the orientation of the AFM-z phase within the monolayer frame (see Fig. S7). In model III, we consider the two lowest magnetic phases: AFM-z and AFM-N [68], assuming the lattice parameters extracted

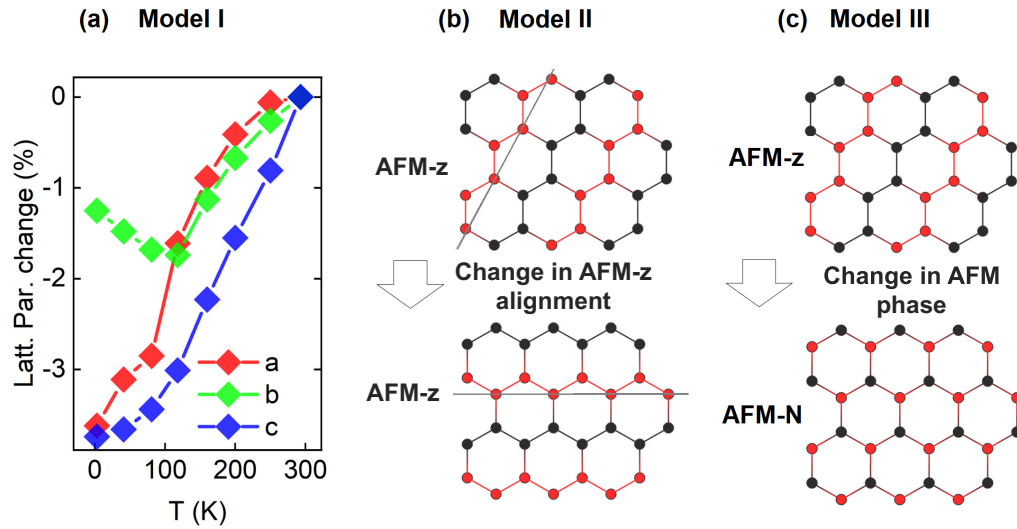


FIG. 4. The impact of three different factors on the dielectric properties are examined. In model I, various lattice parameters are adopted from the XRD measurements (Ref. [58]). In models II and III, the change of the AFM-z orientation and two lowest magnetic phases are assumed, respectively.

from experimental measurements around the kink (~ 50 K). The results of all three models are collected in Table I.

In model I, the changes of the in-plane dielectric contributions are small upon the changes of the lattice parameters. Albeit, there is a visible kink in ionic contribution at 80 K for $U = 5.3$ eV [see Figs. S7(c) and S7(d)], however, it is not shown for other Hubbard U parameter [see Figs. S7(a) and S7(c) for $U = 2.6$ eV]. In model II, the change in the alignment of AFM-z order implies a larger increase of the ionic relative dielectric contribution $\delta\epsilon_{\text{ion}}$ (0.6%) compared to model I (0.3%–0.5%). The strongest changes of in-plane dielectric properties (around 8%, see table) are exposed by the change of the magnetic phases AFM-z and AFM-N. In particular, the largest values of dielectric in-plane constants are obtained for the AFM-N phase. In addition, our results re-

veal that the magnetic ground state (AFM-z) is robust against the employed range of lattice parameters [Fig. S7(b)], in line with recent theoretical reports for the other MPX_3 antiferromagnetic structures [68]. Although the relative change of the magnetic phase is plausible to be observed at higher temperatures (>50 K), as indicated by our DFT+ U results (see explanation in the SM), no significant kinks, jumps, or changes of the in-plane dielectric properties are visible for the Néel temperature at 120 K. In addition, the relative changes of the in-plane contributions (around 3–5%), are rather large in comparison to the experimentally observed ones (0.8%–1%). Hence, model III can be excluded as being the origin of the jump around 50 K. On the other hand, the structural in-plane anisotropy reported recently [66], and the changes in lattice parameters [58] impose a preferred

TABLE I. In-plane contribution of the relative dielectric constants defined as $\delta\epsilon_{\parallel} = (\epsilon_{\parallel} - \epsilon_{\text{ref}})/\epsilon_{\text{ref}}$. In particular, for model I, ϵ_{ref} is taken as a minimal value from the range 3–81 K. Regarding, the total contribution of $\delta\epsilon_0$, each value of ϵ_{\parallel} , $\epsilon_{\parallel}^{\text{ref}}$ is the sum of the ionic and electronic contributions, and thus $\delta\epsilon_0$ is not a sum of $\delta\epsilon_{\infty} + \delta\epsilon_{\text{ion}}$. In the last row, the energy difference ΔE and its corresponding thermal energy is presented. In the case of model I, ΔE is evaluated for the magnetic ground state (AFM-z), in model II, 5.6 meV is taken from Ref. [66] (see SM therein); and in model III ΔE is between two magnetic phases AFM-z and AFM-N [see Fig. S7(b)].

In-plane dielectric contribution $\delta\epsilon_{\parallel}$ [%]	Model I (change of the lattice parameters)	Model II (change of the AFM-z alignment within the layer)	Model III (change of the magnetic phase)
Ionic $\delta\epsilon_{\text{ion}}$	0.3% ($U = 5.3$ eV) 0.5% ($U = 2.6$ eV)	0.6% ($U = 5.3$ eV)	7.9% ($U = 5.3$ eV) 7.6% ($U = 2.6$ eV)
Electronic $\delta\epsilon_{\infty}$	0.12% ($U = 5.3$ eV) 0.14% ($U = 2.6$ eV)	0.01%	7.9% ($U = 5.3$ eV) 0.9% ($U = 2.6$ eV)
Total $\delta\epsilon_0$	0.2% ($U = 5.3$ eV) 0.1% ($U = 2.6$ eV)	0.2%	5.2% ($U = 5.3$ eV) 3.3% ($U = 2.6$ eV)
Experimental: $\sim 0.8\%$ [see Fig. 3(b), obtained for range (3–70 K)]			
ΔE [meV per magnetic atom] (thermal energy)	1.6 meV (19 K)	5.6 meV [66] (65 K)	11.5 meV for $U = 5.3$ eV, (133 K) 3.9 meV for $U = 2.6$ eV, (45 K)

orientation of the magnetic alignment. The energy difference of 5.6 meV per magnetic ion reported in Ref. [66] (see SM therein) indicate that the thermal energy could rotate the AFM-z alignment at a temperature of around 65 K. The relative change in magnetic alignment imposes the change of the in-plane dielectric contributions equal to $\delta\epsilon_0 = 0.2\%$ (model II), which is in the same order as observed experimentally ($\delta\epsilon_0 = 0.8\%$). Note that the theoretical value obtained within model II could be further enhanced by including the relative changes of the lattice parameters, as indicated by model I. Thus, the prominent jump visible around 50 K for the in-plane measurements of the dielectric permittivity might be attributed to the change of the orientation of the AFM-z phase alignment within the plane, enabled by the in-plane structural anisotropy.

V. CONCLUSIONS

To summarize, we examined the magnetodielectric properties of FePS₃ which show anisotropic behavior in the in-plane and out-of-plane directions, which can be attributed to the contrasting nature of bonding and spin texture in these two geometries. A prominent anomaly in the AFM phase (~ 50 K) is observed in the dielectric spectra, supported by ac susceptibility measurements, has been explained in terms of complex interaction in the domains, which might, in turn, lead to domain-wall movements. Computationally, three plausible

models have been examined. Structural in-plane anisotropy along with the nonequivalent changes in lattice parameters imposes a preferred orientation of the magnetic alignment, leading to a kink in dielectric constant at low temperatures. Tailoring the structural anisotropy in 2D magnets by tuning magnetodielectric coupling may be promising for future spin-logic device applications.

ACKNOWLEDGMENTS

We are grateful to the CSS facility at IACS and Professor S. Giri for support with the dielectric measurements. The authors acknowledge fruitful discussions with Prof. K. Sengupta, Dr. M. Mondal, Dr. K. D. M. Rao, Dr. M. Palit, Mr. S. Das, and Ms. S. Baidya. A.G. thanks Dr. A. Banerjee and S. Mukherjee. M.B. acknowledges support from the University of Warsaw within the project Excellence Initiative-Research University program. Access to computing facilities of PL-Grid Polish Infrastructure for Supporting Computational Science in the European Research Space and of the Interdisciplinary Center of Modeling (ICM), University of Warsaw are gratefully acknowledged. S.M. is grateful to DST-INSPIRE for his fellowship. S.G. acknowledges CSIR for the fellowship (File No. 09/080(1133)/2019-EMR-I). S.D. would like to acknowledge DST-SERB Grant No. CRG/2021/004334 and e-beam lithography facility of TRC at IACS. The authors are also thankful to the facilities at UGC-DAE-CSR-Indore.

-
- [1] R. Dubrovin, N. Siverin, P. Syrnikov, N. Novikova, K. Boldyrev, and R. Pisarev, Lattice dynamics and microscopic mechanisms of the spontaneous magnetodielectric effect in the antiferromagnetic fluoroperovskites KCoF₃ and RbCoF₃, *Phys. Rev. B* **100**, 024429 (2019).
- [2] G. Lawes, A. Ramirez, C. Varma, and M. Subramanian, Magnetodielectric Effects from Spin Fluctuations in Isostructural Ferromagnetic and Antiferromagnetic Systems, *Phys. Rev. Lett.* **91**, 257208 (2003).
- [3] T. Kolodiazny, H. Sakurai, and N. Vittayakorn, Spin-flip driven magneto-dielectric effect in Co₄Nb₂O₉, *Appl. Phys. Lett.* **99**, 132906 (2011).
- [4] T. Aoyama, Y. Hasegawa, S. Kimura, T. Kimura, and K. Ohgushi, Anisotropic magnetodielectric effect in the honeycomb-type magnet α -RuCl₃, *Phys. Rev. B* **95**, 245104 (2017).
- [5] S. Jiang, J. Shan, and K. Mak, Electric-field switching of two-dimensional van der Waals magnets, *Nat. Mater.* **17**, 406 (2018).
- [6] H. Chu, C. Roh, J. Island, C. Li, S. Lee, J. Chen, J. Park, A. Young, J. Lee, and D. Hsieh, Linear Magnetoelectric Phase in Ultrathin MnPS₃ Probed by Optical Second Harmonic Generation, *Phys. Rev. Lett.* **124**, 027601 (2020).
- [7] N. Hill, Why are there so few magnetic ferroelectrics? *J. Phys. Chem. B* **104**, 6694 (2000).
- [8] G. Catalan, Magnetocapacitance without magnetoelectric coupling, *Appl. Phys. Lett.* **88**, 102902 (2006).
- [9] D. Choudhury, P. Mandal, R. Mathieu, A. Hazarika, S. Rajan, A. Sundaresan, U. Waghmare, R. Knut, O. Karis, P. Nordblad, and D. Sharma, Near-room-temperature Colossal Magnetodielectricity and Multiglass Properties in Partially Disordered La₂NiMnO₆, *Phys. Rev. Lett.* **108**, 127201 (2012).
- [10] W. Eerenstein, N. Mathur, and J. Scott, Multiferroic and magnetoelectric materials, *Nature (London)* **442**, 759 (2006).
- [11] S.-P. Shen, J.-C. Wu, J.-D. Song, X.-F. Sun, Y.-F. Yang, Y.-S. Chai, D.-S. Shang, S.-G. Wang, J. F. Scott, and Y. Sun, Quantum electric-dipole liquid on a triangular lattice, *Nat. Commun.* **7**, 10569 (2016).
- [12] T. Kimura, S. Kawamoto, I. Yamada, M. Azuma, M. Takano, and Y. Tokura, Magnetocapacitance effect in multiferroic BiMnO₃, *Phys. Rev. B* **67**, 180401(R) (2003).
- [13] M. Singh, K. Truong, and P. Fournier, Magnetodielectric effect in double perovskite La₂CoMnO₆ thin films, *Appl. Phys. Lett.* **91**, 042504 (2007).
- [14] J. Lee, L. Fang, E. Vlahos, X. Ke, Y. Jung, L. Kourkoutis, J. Kim, P. Ryan, T. Heeg, M. Roeckerath and Others, A strong ferroelectric ferromagnet created by means of spin-lattice coupling, *Nature (London)* **466**, 954 (2010).
- [15] R. Clement, L. Lomas, and J. Audiere, Intercalation chemistry of layered iron trithiophosphate (FePS₃). An approach toward insulating magnets below 90 K, *Chem. Mater.* **2**, 641 (1990).
- [16] L. Silipigni, L. Schirò, T. Quattrone, V. Grasso, G. Salvato, L. Monsù Scolaro, and G. De Luca, Dielectric spectra of manganese thiophosphate intercalated with sodium ions, *J. Appl. Phys.* **105**, 123703 (2009).
- [17] A. Ghosh, M. Palit, S. Maity, V. Dwij, S. Rana, and S. Datta, Spin-phonon coupling and magnon scattering in few-layer antiferromagnetic FePS₃, *Phys. Rev. B* **103**, 064431 (2021).

- [18] See Supplemental Material at <http://link.aps.org/supplemental/10.1103/PhysRevB.108.L060403> for the details of growth, computational methods, and other discussions, which includes Refs. [19–37].
- [19] A. Castellanos-Gomez, M. Buscema, R. Molenaar, V. Singh, L. Janseen, H. Van Der Zant, and G. Steele, Deterministic transfer of two-dimensional materials by all-dry viscoelastic stamping, *2D Mater.* **1**, 011002 (2014).
- [20] G. Kresse and J. Hafner, *Ab initio* molecular dynamics for liquid metals, *Phys. Rev. B* **47**, 558(R) (1993).
- [21] G. Kresse and J. Furth Müller, Efficiency of ab-initio total energy calculations for metals and semiconductors using a plane-wave basis set, *Comput. Mater. Sci.* **6**, 15 (1996).
- [22] S. L. Dudarev, G. A. Bottom, S. Y. Savrasov, C. J. Humphreys, and A. P. Sutton, Electron-energy-loss spectra and the structural stability of nickel oxide: An LSDA+U study, *Phys. Rev. B* **57**, 1505 (1998).
- [23] S. Grimme, J. Antony, S. Ehrlich, and H. Krieg, A consistent and accurate ab initio parametrization of density functional dispersion correction (DFT-D) for the 94 elements H-Pu, *J. Chem. Phys.* **132**, 154104 (2010).
- [24] M. Birowska, P. E. Faria Junior, J. Fabian, and J. Kuntsmann, Large exciton binding energies in MnPS₃ as a case study of a van der Waals layered magnet, *Phys. Rev. B* **103**, L121108 (2021).
- [25] G. Ouvrard, R. Brec, and J. Rouxel, Structural determination of some MPS₃ layered phases (M = Mn, Fe, Co, Ni and Cd), *Mater. Res. Bull.* **20**, 1181 (1985).
- [26] M. Gajdoš, K. Hummer, G. Kresse, J. Furthmüller, and F. Bechstedt, Linear optical properties in the projector-augmented wave methodology, *Phys. Rev. B* **73**, 045112 (2006).
- [27] A. Von Hippel, *Dielectrics and Waves* (MIT Press, Cambridge, MA, 1966).
- [28] A. Jonscher, *Dielectric Relaxation in Solids* (Chelsea Dielectrics Press, London, 1983).
- [29] K. Neupane, J. Cohn, H. Terashita, and J. Neumeier, Doping dependence of polaron hopping energies in La_{1-x}Ca_xMnO₃ (0 ≤ x ≤ 0.15), *Phys. Rev. B* **74**, 144428 (2006).
- [30] A. Wildes, D. Lançon, M. Chan, F. Weickert, N. Harrison, V. Simonet, M. Zhitomirsky, M. Gvozdikova, T. Ziman, and H. Rønnow, High field magnetization of FePS₃, *Phys. Rev. B* **101**, 024415 (2020).
- [31] E. Chudnovsky, D. Garanin, and R. Schilling, Universal mechanism of spin relaxation in solids, *Phys. Rev. B* **72**, 094426 (2005).
- [32] E. Chudnovsky and D. Garanin, Phonon Superradiance and Phonon Laser Effect in Nanomagnets, *Phys. Rev. Lett.* **93**, 257205 (2004).
- [33] B. Shih, Y. Xue, P. Zhang, M. Cohen, and S. Louie, Quasiparticle Band Gap of ZnO: High Accuracy from the Conventional G0W0 Approach, *Phys. Rev. Lett.* **105**, 146401 (2010).
- [34] H. Cao, Z. Yu, P. Lu, and L. Wang, Fully converged plane-wave-based self-consistent GW calculations of periodic solids, *Phys. Rev. B* **95**, 035139 (2017).
- [35] C. Lane and J.-X. Zhu, Thickness dependence of electronic structure and optical properties of a correlated van der Waals antiferromagnetic NiPS₃ thin film, *Phys. Rev. B* **102**, 075124 (2020).
- [36] K. Kim, S. Y. Lim, J.-U. Lee, S. Lee, T. Y. Kim, K. Park, G. S. Jeon, C.-H. Park, J.-G. Park, and H. Cheong, Suppression of magnetic ordering in XXZ-type antiferromagnetic monolayer NiPS₃, *Nat. Commun.* **10**, 345 (2019).
- [37] Y. Takano, A. Arai, Y. Takahashi, K. Takase, and K. Sekizawa, Magnetic properties and specific heat of new spin glass Mn_{0.5}Fe_{0.5}PS₃, *J. Appl. Phys.* **93**, 8197 (2003).
- [38] K. Kao, *Dielectric Phenomena in Solids* (Elsevier Academic Press, San Diego, CA, 2004).
- [39] S. Chanda, S. Saha, A. Dutta, J. Krishna Murthy, A. Venimadhav, S. Shannigrahi, and T. Sinha, Magnetic ordering and conduction mechanism of different electroactive regions in Lu₂NiMnO₆, *J. Appl. Phys.* **120**, 134102 (2016).
- [40] N. Mott and E. Davis, *Electronic Processes in Non-crystalline Materials* (Oxford University Press, Oxford, 2012).
- [41] X. Chen, C. Zhang, C. Almasan, J. Gardner, and J. Sarrao, Small-polaron hopping conduction in bilayer manganite La_{1.2}Sr_{1.8}Mn₂O₇, *Phys. Rev. B* **67**, 094426 (2003).
- [42] A. Karmakar, S. Majumdar, and S. Giri, Polaron relaxation and hopping conductivity in LaMn_{1-x}Fe_xO₃, *Phys. Rev. B* **79**, 094406 (2009).
- [43] D. Joung, and S. Khondaker, Efros-Shklovskii variable-range hopping in reduced graphene oxide sheets of varying carbon *sp*² fraction, *Phys. Rev. B* **86**, 235423 (2012).
- [44] T. Holstein, Studies of polaron motion: Part II. The small polaron, *Ann. Phys.* **8**, 343 (1959).
- [45] M. Seehra and R. Helmick, Anomalous changes in the dielectric constants of MnF₂ near its Néel temperature, *J. Appl. Phys.* **55**, 2330 (1984).
- [46] P. Joy and S. Vasudevan, Infrared (700-100 cm⁻¹) vibrational spectra of the layered transition metal thiophosphates, MPS₃ (M= Mn, Fe and Ni), *J. Phys. Chem. Solids* **54**, 343 (1993).
- [47] Z. L. Sun *et al.*, Field-induced metal-to-insulator transition and colossal anisotropic magnetoresistance in a nearly Dirac material EuMnSb₂, *npj Quantum Mater.* **6**, 94 (2021).
- [48] D. Gong, S. Huang, F. Ye, X. Gui, J. Zhang, W. Xie, and R. Jin, Canted Eu magnetic structure in EuMnSb₂, *Phys. Rev. B* **101**, 224422 (2020).
- [49] X.-X. Zhang, S. Jiang, J. Lee, C. Lee, K. F. Mak, and J. Shan, Spin dynamics slowdown near the antiferromagnetic critical point in atomically thin FePS₃, *Nano Lett.* **21**, 5045 (2021).
- [50] D. Vaclavkova, M. Palit, J. Wyzula, S. Ghosh, A. Delhomme, S. Maity, P. Kapuscinski, A. Ghosh, M. Veis, M. Grzeszczyk and Others, Magnon polarons in the van der Waals antiferromagnet FePS₃, *Phys. Rev. B* **104**, 134437 (2021).
- [51] J. W. Simonson *et al.*, Magnetic and structural phase diagram of CaMn₂Sb₂, *Phys. Rev. B* **86**, 184430 (2012).
- [52] Y. Park, K. Song, K. Lee, C. Won, and N. Hur, Effect of antiferromagnetic order on the dielectric properties of Bi₂Fe₄O₉, *Appl. Phys. Lett.* **96**, 092506 (2010).
- [53] F. Schrettle, S. Krohns, P. Lunkenheimer, J. Hemberger, N. Büttgen, H. Von Nidda, A. Prokofiev, and A. Loidl, Switching the ferroelectric polarization in the S= 1/2 chain cuprate LiCuVO₄ by external magnetic fields, *Phys. Rev. B* **77**, 144101 (2008).
- [54] F. Schrettle, S. Krohns, P. Lunkenheimer, V. Brabers, and A. Loidl, Relaxor ferroelectricity and the freezing of short-range polar order in magnetite, *Phys. Rev. B* **83**, 195109 (2011).
- [55] J. Shi, M. Johnson, M. Zhang, P. Gao, and M. Jain, Antiferromagnetic and dielectric behavior in polycrystalline GdFe_{0.5}Cr_{0.5}O₃ thin film, *APL Mater.* **8**, 031106 (2020).

- [56] S. Krohns and P. Lunkenheimer, Ferroelectric polarization in multiferroics, *Phys. Sci. Rev.* **4**, 20190015 (2019).
- [57] D. Evans, M. Alexe, A. Schilling, A. Kumar, D. Sanchez, N. Ortega, R. Katiyar, J. Scott, and J. Gregg, The nature of magnetoelectric coupling in $\text{Pb}(\text{Zr}, \text{Ti})\text{O}_3\text{-Pb}(\text{Fe}, \text{Ta})\text{O}_3$, *Adv. Mater.* **27**, 6068 (2015).
- [58] C. Murayama, M. Okabe, D. Urushihara, T. Asaka, K. Fukuda, M. Isobe, K. Yamamoto, and Y. Matsushita, Crystallographic features related to a van der Waals coupling in the layered chalcogenide FePS_3 , *J. Appl. Phys.* **120**, 142114 (2016).
- [59] D. Lançon, H. Walker, E. Ressouche, B. Ouladdiaf, K. Rule, G. McIntyre, T. Hicks, H. Rønnow, and A. Wildes, Magnetic structure and magnon dynamics of the quasi-two-dimensional antiferromagnet FePS_3 , *Phys. Rev. B* **94**, 214407 (2016).
- [60] A. K. Budniak, S. J. Zelewski, M. Birowska, T. Woźniak, T. Bendikov, Y. Kauffmann, Y. Amouyal, R. Kudrawiec, and E. Lifshitz, Spectroscopy and structural investigation of iron phosphorus trisulfide- FePS_3 , *Adv. Opt. Mater.* **10**, 2102489 (2022).
- [61] P. Jernberg, S. Bjarman, and R. Wäppling, FePS_3 : A first-order phase transition in a “2D” Ising antiferromagnet, *J. Magn. Mater.* **46**, 178 (1984).
- [62] M. Nauman, D. Kiem, S. Lee, S. Son, J. Park, W. Kang, M. Han, and Y. Jo, Complete mapping of magnetic anisotropy for prototype Ising van der Waals FePS_3 , *2D Mater.* **8**, 035011 (2021).
- [63] C. Sarkis, S. Säubert, V. Williams, E. Choi, T. Reeder, H. Nair, and K. Ross, Low-temperature domain-wall freezing and nonequilibrium dynamics in the transverse-field Ising model material CoNb_2O_6 , *Phys. Rev. B* **104**, 214424 (2021).
- [64] D. Abdul-Wahab, E. Iacocca, R. Evans, A. Bedoya-Pinto, S. Parkin, K. Novoselov, and E. Santos, Domain wall dynamics in two-dimensional van der Waals ferromagnets, *Appl. Phys. Rev.* **8**, 041411 (2021).
- [65] I. Alliat, R. Evans, K. Novoselov, and E. Santos, Relativistic domain-wall dynamics in van der Waals antiferromagnet MnPS_3 , *npj Comput. Mater.* **8**, 3 (2022).
- [66] E. Geraffy, S. Zuri, M. M. Rybak, F. Horani, A. K. Budniak, Y. Amouyal, M. Birowska, and E. Lifshitz, Crystal anisotropy implications on the intrinsic magnetic and optical properties in van der Waals FePS_3 , [arXiv:2208.10890](https://arxiv.org/abs/2208.10890).
- [67] M. Amirabbasi and P. Kratzer, Orbital and magnetic ordering in single-layer FePS_3 : A DFT+U study, *Phys. Rev. B* **107**, 024401 (2023).
- [68] C. Autieri, G. Cuono, C. Noce, M. Rybak, K. Kotur, C. Agrapidis, K. Wohlfeld, and M. Birowska, Limited Ferromagnetic Interactions in Monolayers of MPS_3 ($\text{M} = \text{Mn}$ and Ni), *J. Phys. Chem. C* **126**, 6791 (2022).